www.sciencemag.org/cgi/content/full/science.1241681/DC1

Supplementary Materials for

In Situ Observations of Interstellar Plasma With Voyager 1

D. A. Gurnett,* W. S Kurth, L. F. Burlaga, N. F. Ness

*Corresponding author. E-mail: donald-gurnett@uiowa.edu

Published 12 September 2013 on *Science* Express
DOI: 10.1126/science.1241681

This PDF file includes:

Text S1 Material:

Electron plasma oscillations.

If a slab of electrons is displaced from its equilibrium position, the resulting polarization charge produces an electric field that acts to pull the electrons back to their original position. It is easily shown that the restoring force is directly proportional to the displacement *(16)*, i.e., Hooke's law, which means that when released the electrons oscillate at a constant frequency around their equilibrium position. If the electric field has a sufficiently long wavelength, the oscillation is at a characteristic frequency called the electron plasma frequency, $\omega_p = [n_e^2 e^2/\varepsilon_0 m_e]^{1/2}$, where n_e is the electron number density, e is the electronic charge, ε_0 is the permittivity of free space, and m_e is the electron mass. It is also easily shown that the electric field is purely electrostatic, i.e., derivable from a potential, and although there is an oscillating current, no magnetic field is produced by the electron motion (the displacement current cancels the conduction current). As the wavelength decreases the electron pressure gradient force begins to be important and the oscillation frequency, ω, shifts above ω_p, by an amount that depends on the wavelength. In this regime, where electron pressure is important, it is customary to call the resulting oscillations Langmuir waves, after Tonks and Langmuir *(34)* who first studied these oscillations. The oscillation frequency is then given by the Bohm and Gross *(35)* dispersion relation, $\omega^2 = \omega_p^2[1 + 3(k\lambda_D)^2]$, where $k = 2\pi/\lambda$ is the wave number, λ is the wavelength, $\lambda_D = [\varepsilon_0 \kappa T_e/n_e e^2]^{1/2}$ is the Debye length, T_e is the electron temperature, and κ is Boltzmann's constant. The minimum wavelength is determined by a collisionless damping process called Landau damping *(16)* that becomes very strong near $k\lambda_D = 1$. Because of this damping Langmuir waves can only occur for wavelengths such that $k\lambda_D << 1$. Therefore, Langmuir waves are usually confined to frequencies not more than a few percent above the electron plasma frequency.

Excitation.

Langmuir waves are excited by three processes: thermal fluctuations, beam-driven instabilities, and parametric decay. Thermally excited Langmuir wave fluctuations are always present in a plasma and occur in a very narrow band of frequencies around ω_p. These waves are extremely weak, less than a μV/m for densities of ~0.1 cm^{-3} and temperatures of 10^4 to 10^5 K, and require excellent sensitivity to detect. For the very short electric antenna used by the PWS (fig. S2), which has an effective length of only 7m, thermally excited Langmuir waves usually cannot be detected. However, when a sufficiently intense electron beam is present the Langmuir mode can become unstable. The thermally excited plasma oscillations then grow exponentially to very large amplitudes. The basic condition for instability *(16)* is that the electron distribution function must have a region of positive slope, $\partial f/\partial v$, at or near the beam velocity, V_b. Ion beams can in principle drive an instability, but this is extremely rare. In the region of positive slope the wave grows at a phase velocity that matches the beam velocity, i.e., $\omega/k \approx V_b$. For beam-induced growth to exceed the Landau damping, the beam velocity must be well above the electron thermal speed, $V_e = [\kappa T_e/m_e]^{1/2}$. Langmuir waves often have very irregular, spiky intensity variations. These spiky intensity variations arise because of the very rapid exponential growth that occurs as soon as the beam exceeds the instability threshold. The exponential growth makes the electric field intensity extremely sensitive to small fluctuations in the various parameters that control the onset of the instability, such as the beam velocity and plasma density.

Text S2 Material

Comparison of electric and magnetic field directions.

Two roll maneuvers, one in support of the MAG instrument and the other in support of the LECP instrument, were performed during the April-May 2013 period that allowed us to compare the direction of the electric field oscillations to the magnetic field direction. Both were performed by rolling the spacecraft around the spacecraft Z axis, see Fig. S2. Since the -Z axis is directed toward the Sun, which is within 0.5˚ of the direction to Earth, for purposes of analyzing the electric field direction we assume that the effective electric antenna axis, which is along the spacecraft X axis, is rotating in the **T-N** plane of the (R,T,N) coordinate system.

MAG roll

The first roll maneuver that we analyzed was on day 122, 2013. This maneuver consisted of ten rotations to calibrate the MAG instrument. The maneuver started at 14:12:49 UT and ended at 19:47:38 UT on the same day. Although the electric field strength in the 3.11 kHz channel was relatively low during this time, see Fig. 1, a very clear roll modulation pattern was observed, with sharp nulls at roll angles of $\varphi = 64.8^\circ$ and 244.8˚, see the top panel of Fig. 4. Since the electric antenna detects the projection of the electric field onto the antenna axis, these sharp nulls indicate that the electric field is perpendicular to the electric antenna axis at these times, exactly as one would expect for a linearly polarized electrostatic oscillation. No information can be obtained about the Z component of the electric field. A fit of $\left|\cos(\varphi - \varphi_E)\right|$ to the measured electric fields shows that the direction of the electric field oscillation is at an angle of $\varphi_E = 154.8^\circ$ (or 334.8˚) measured counterclockwise with respect to the **+T** axis, as viewed from the **+R** direction, see the top panel of Fig. 4. The statistical uncertainty in the fit is $\Delta\varphi_E = \pm 1.9^\circ$. There is an additional systematic source of error in determining the actual roll start/stop times that we estimate is about 3 degrees, or less. The magnetic field in (R,T,N) coordinates averaged over the duration of the maneuver was (0.1459, -0.4526, 0.2037) nT, and the corresponding direction of the magnetic field projected onto the **T-N** plane was $\varphi_B = 155.8^\circ$, with an uncertainty of about $\Delta\varphi_B = \pm 3^\circ$. The difference between the electric and magnetic field directions is then $\varphi_E - \varphi_B = -1.0^\circ$, which is remarkably small, significantly smaller than the uncertainty in both the electric and magnetic field directions.

LECP roll

The second roll maneuver that we analyzed was on day 120, 2013. This maneuver consisted of a single rotation that was designed to provide special viewing directions for the LECP instrument. The maneuver started at 05:14:54 UT and was performed in three segments ending at 10:04:27 UT on the same day. Although the roll was performed in three segments, with the second segment being a long, 4h 16m hesitation at a roll angle of 70˚, a very clear modulation pattern was observed, with sharp nulls at a roll angles of $\varphi = 68.2^\circ$ and 248.2˚, see the bottom panel of Fig. 4. A fit of $\left|\cos(\varphi - \varphi_E)\right|$ to the measured electric fields shows that the direction of the electric field oscillation is at an angle of $\varphi_E = 158.2^\circ$ (or 338.2˚). The statistical uncertainty in the fit is $\pm 0.5^\circ$. Since the magnetic field could not be accurately measured during the roll maneuver, we averaged the magnetic field components immediately before and after the maneuver, which were very nearly the same. The average magnetic field in (R,T,N) coordinates was (0.177, -0.422, 0.197) nT, and the corresponding direction of the magnetic field projected onto the **T-N** plane was $\varphi_B = 155.0^\circ$, with an uncertainty of about $\Delta\varphi_B = \pm 3^\circ$. The difference

between the electric and magnetic field directions is then $\varphi_E - \varphi_B = 3.2^\circ$, which is a little larger than during the MAG roll, but still comparable to the uncertainty in the measurement.

Fig. S1: The heliosphere and Voyagers 1 and 2.

This sketch shows the definitions used in this paper for the three main plasma regions around the Sun. These consist of (a) the solar wind, which extends from the Sun to the termination shock; (b) the heliosheath, which is shock-heated solar plasma that extends from the termination shock to the heliopause; and (c) the interstellar plasma, which is approaching the Sun at a speed of 23 km/s *(36)*. The view in this sketch is from along the ecliptic plane perpendicular to the interstellar plasma flow. Sometimes a bow shock is shown in the interstellar plasma flow *(1,2)*, in which case the region between the termination shock and the heliopause is called the inner heliosheath, and the region between the heliopause and the bow shock is called the outer heliosheath. However, recent IBEX measurements *(36)* show that the interstellar plasma flow is too slow to produce a shock in the interstellar plasma flow, so no bow shock is shown. As shown the Voyager spacecraft are moving outward more or less toward the nose of the heliopause. Voyager 1 is currently at a heliocentric radial distance of 125 AU (1 AU = 1.49 x 10^8 km) and a heliographic latitude and longitude of 34.6º and 174.2º, and Voyager 2 is currently at a radial distance of 102 AU and a heliographic latitude and longitude of -30º and 217º.

Fig. S2: The Voyager spacecraft and the PWS antenna.

A drawing of the Voyager spacecraft that shows the PWS electric field antennas. The PWS uses the two monopole antenna elements as a dipole (i.e., responds to the voltage difference, $V_1 - V_2$), which means that the effective axis of the antenna is between the center of the two elements, parallel to the X-axis of the spacecraft. Roll maneuvers are performed around the Z axis of the spacecraft. The Z axis is always along the Earth-spacecraft line to keep the high gain antenna pointed toward Earth. Because of the great distance from the Sun, the Earth-spacecraft line is very close to the Sun-spacecraft line. This means that the Z axis of the spacecraft is very nearly parallel to the **R** vector in the (R,T,N) coordinates system shown in Fig. 4. In this coordinate system **R** is a radial vector from the Sun to the spacecraft, **T** is an azimuthal vector perpendicular to the rotational axis of the Sun, and **N** completes the right-hand system.

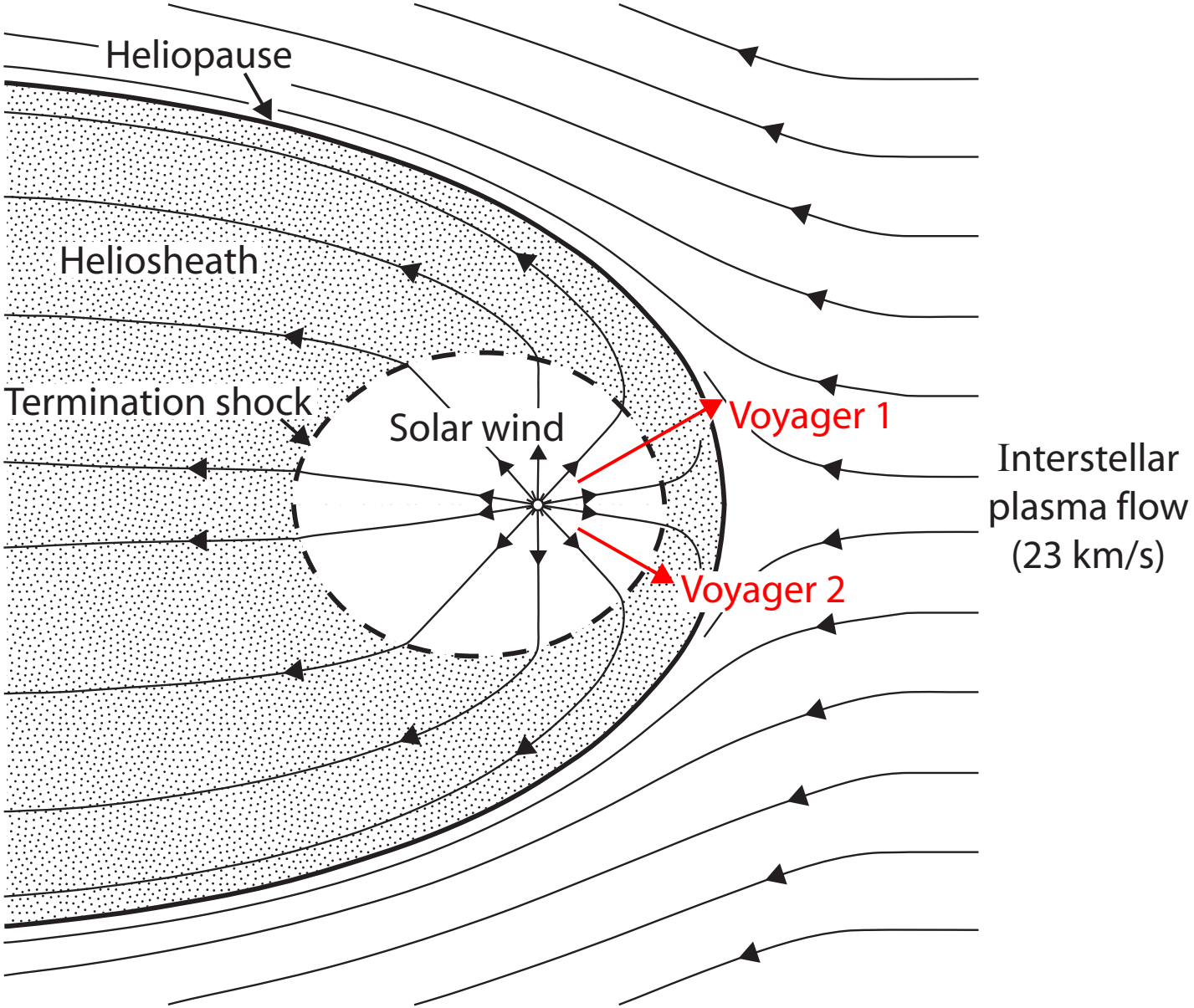
Heliopause
Heliosheath
Termination shock
Solar wind
Voyager 1
Voyager 2
Interstellar
plasma flow
(23 km/s)

C-D82-478-1

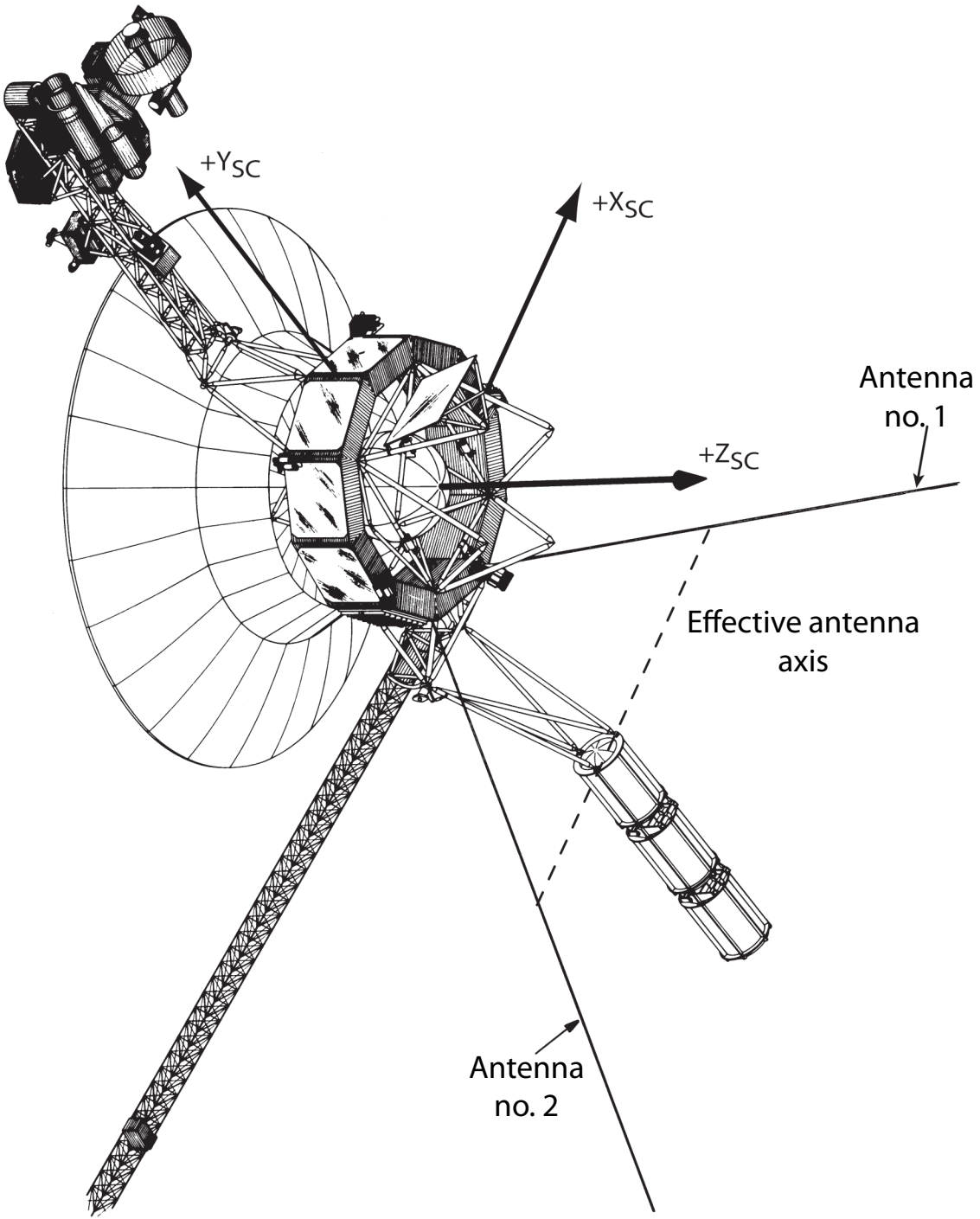

References and Notes

1. W. I. Axford, in *Physics of the Outer Heliosphere*, S. Grzedzielski, D. E. Page, Eds. (Pergamon, Oxford, 1990), pp. 7–15.

2. G. P. Zank, Interaction of the solar wind with the local interstellar medium: a theoretical perspective. *Space Sci. Rev.* **89**, 413–688 (1999). doi:10.1023/A:1005155601277

3. L. F. Burlaga, N. F. Ness, M. H. Acuña, R. P. Lepping, J. E. Connerney, E. C. Stone, F. B. McDonald, Crossing the termination shock into the heliosheath: Magnetic fields. *Science* **309**, 2027–2029 (2005). Medline doi:10.1126/science.1117542

4. L. F. Burlaga, N. F. Ness, M. H. Acuña, R. P. Lepping, J. E. Connerney, J. D. Richardson, Magnetic fields at the solar wind termination shock. *Nature* **454**, 75–77 (2008). Medline doi:10.1038/nature07029

5. D. A. Gurnett, W. S. Kurth, Electron plasma oscillations upstream of the solar wind termination shock. *Science* **309**, 2025–2027 (2005). Medline doi:10.1126/science.1117425

6. D. A. Gurnett, W. S. Kurth, Intense plasma waves at and near the solar wind termination shock. *Nature* **454**, 78–80 (2008). Medline doi:10.1038/nature07023

7. W. R. Webber, F. B. McDonald, Recent Voyager 1 data indicate that on 25 August 2012 at a distance of 121.7 AU from the Sun, sudden and unprecedented intensity changes were observed in anomalous and galactic cosmic rays. *Geophys. Res. Lett.* **40**, 1665–1668 (2013). doi:10.1002/grl.50383

8. E. C. Stone *et al*., Voyager 1 observes low-energy galactic cosmic rays in a region depleted of heliospheric ions. *Science* **341**, 150–153 (2013).

9. S. M. Krimigis, R. B. Decker, E. C. Roelof, M. E. Hill, T. P. Armstrong, G. Gloeckler, D. C. Hamilton, L. J. Lanzerotti, Search for the Exit: Voyager 1 at heliosphere's border with the Galaxy. *Science* **341**, 144–147 (2013). doi:10.1126/science.1235721

10. E. C. Stone, A. C. Cummings, F. B. McDonald, B. C. Heikkila, N. Lal, W. R. Webber, Voyager 1 explores the termination shock region and the heliosheath beyond. *Science* **309**, 2017–2020 (2005). Medline doi:10.1126/science.1117684

11. R. B. Decker, S. M. Krimigis, E. C. Roelof, M. E. Hill, T. P. Armstrong, G. Gloeckler, D. C. Hamilton, L. J. Lanzerotti, Voyager 1 in the foreshock, termination shock, and heliosheath. *Science* **309**, 2020–2024 (2005). Medline doi:10.1126/science.1117569

12. L. F. Burlaga, N. F. Ness, E. C. Stone, Magnetic field observations as Voyager 1 entered the heliosheath depletion region. *Science* **341**, 147–150 (2013). doi:10.1126/science.1235451

13. P. C. Frisch, S. Redfield, J. D. Slavin, The interstellar medium surrounding the Sun. *Annu. Rev. Astron. Astrophys.* **49**, 237–279 (2011). doi:10.1146/annurev-astro-081710-102613

14. D. J. McComas, H. O. Funsten, S. A. Fuselier, W. S. Lewis, E. Möbius, N. A. Schwadron, IBEX observations of heliospheric energetic neutral atoms: Current understanding and future directions. *Geophys. Res. Lett.* **38**, L18101 (2011). doi:10.1029/2011GL048763

15. F. L. Scarf, D. A. Gurnett, A plasma wave investigation for the Voyager Mission. *Space Sci. Rev.* **21**, 289 (1977). doi:10.1007/BF00211543

16. D. A. Gurnett, A. Bhattacharjee, in *Introduction to Plasma Physics with Space and Laboratory Applications* (Cambridge Univ. Press, Cambridge, 2005), p. 11.

17. I. H. Cairns, P. A. Robinson, Theory for low-frequency modulated Langmuir wave packets. *Geophys. Res. Lett.* **19**, 2187–2190 (1992). doi:10.1029/92GL02632

18. R. E. Ergun, D. M. Malaspina, I. H. Cairns, M. V. Goldman, D. L. Newman, P. A. Robinson, S. Eriksson, J. L. Bougeret, C. Briand, S. D. Bale, C. A. Cattell, P. J. Kellogg, M. L. Kaiser, Eigenmode structure in solar-wind Langmuir waves. *Phys. Rev. Lett.* **101**, 051101 (2008). Medline doi:10.1103/PhysRevLett.101.051101

19. D. A. Gurnett, W. S. Kurth, S. C. Allendorf, R. L. Poynter, Radio emission from the heliopause triggered by an interplanetary shock. *Science* **262**, 199–203 (1993). Medline doi:10.1126/science.262.5131.199

20. W. S. Kurth, D. A. Gurnett, F. L. Scarf, R. L. Poynter, Detection of a radio emission at 3 kHz in the outer heliosphere. *Nature* **312**, 27–31 (1984). doi:10.1038/312027a0

21. G. P. Zank, H.-R. Müller, The dynamical heliosphere. *J. Geophys. Res.* **108**, 1240 (2003). doi:10.1029/2002JA009689

22. W. S. Kurth, D. A. Gurnett, On the source location of low-frequency heliospheric radio emissions. *J. Geophys. Res.* **108**, 8027 (2003). doi:10.1029/2003JA009860

23. H. Washimi, W. Webber, G. P. Zank, Q. Hu, V. Florinski, J. Adams, Y. Kubo, A role of magnetosonic pulses on variations of *Voyager-1* MeV electron intensity in the heliosheath. *Astrophys. J.* **757**, L2 (2012). doi:10.1088/2041-8205/757/1/L2

24. M. Guhathakurta, Interplanetary Space Weather: A New Paradigm. *Eos* **94**, 165–166 (2013). doi:10.1002/2013EO180001

25. S. D. Bale, M. J. Reiner, J.-L. Bougeret, M. L. Kaiser, S. Krucker, D. E. Larson, R. P. Lin, The source region of an interplanetary type II radio burst. *Geophys. Res. Lett.* **26**, 1573–1576 (1999). doi:10.1029/1999GL900293

26. J. D. Richardson, C. Wang, *Voyager 2* observes a large density increase in the heliosheath. *Astrophys. J.* **759**, L19 (2012). doi:10.1088/2041-8205/759/1/L19

27. http://web.mit.edu/afs/athena/org/s/space/www/voyager.html.

28. G. P. Zank, J. Heerikhuisen, B. E. Wood, N. V. Pogorelov, E. Zirnstein, D. J. McComas, Heliospheric structure: The bow wave and the hydrogen wall. *Astrophys. J.* **763**, 20 (2013). doi:10.1088/0004-637X/763/1/20

29. N. V. Pogorelov, G. P. Zank, T. Ogino, Three-dimensional features of the outer heliosphere due to coupling between the interstellar and interplanetary magnetic fields. II. The presence of neutral hydrogen atoms. *Astrophys. J.* **644**, 1299–1316 (2006). doi:10.1086/503703

30. H. Washimi, G. P. Zank, Q. Hu, T. Tanaka, K. Munakata, H. Shinagawa, Realistic and time-varying outer heliospheric modelling. *Mon. Not. R. Astron. Soc.* **416**, 1475–1485 (2011). doi:10.1111/j.1365-2966.2011.19144.x

31. J. D. Richardson, J. C. Kasper, C. Wang, J. W. Belcher, A. J. Lazarus, Cool heliosheath plasma and deceleration of the upstream solar wind at the termination shock. *Nature* **454**, 63–66 (2008). Medline doi:10.1038/nature07024

32. J. F. Drake, M. Opher, M. Swisdak, J. N. Chamoun, A magnetic reconnection mechanism for the generation of anomalous cosmic rays. *Astrophys. J.* **709**, 963 (2010). doi:10.1088/0004-637X/709/2/963

33. V. Florinski, G. P. Zank, N. V. Pogorolov, Heliopause stability in the presence of neutral atoms: Rayleigh-Taylor dispersion analysis and axisymmetric MHD simulations. *J. Geophys. Res.* **110**, A07104 (2005). doi:10.1029/2004JA010879

34. L. Tonks, I. Langmuir, Oscillations in ionized gases. *Phys. Rev.* **33**, 195–210 (1929). doi:10.1103/PhysRev.33.195

35. D. Bohm, E. P. Gross, Theory of plasma oscillations. A. Origin of medium-like behavior. *Phys. Rev.* **75**, 1851–1864 (1949). doi:10.1103/PhysRev.75.1851

36. D. J. McComas, D. Alexashov, M. Bzowski, H. Fahr, J. Heerikhuisen, V. Izmodenov, M. A. Lee, E. Möbius, N. Pogorelov, N. A. Schwadron, G. P. Zank, The heliosphere's interstellar interaction: No bow shock. *Science* **336**, 1291–1293 (2012). Medline doi:10.1126/science.1221054